

# Hard x-ray 1s photoemission spectroscopy as a probe of charge transfer in late transition metal oxides

Mahnaz Ghiasi,<sup>1</sup> Atsushi Hariki,<sup>2</sup> Mathias Winder,<sup>2</sup> Jan Kuneš,<sup>2,3</sup> Anna Regoutz,<sup>4</sup>  
Tien-Lin Lee,<sup>5</sup> Yongfeng Hu,<sup>6</sup> Jean-Pascal Rueff,<sup>7,8</sup> and Frank M. F. de Groot<sup>1</sup>

<sup>1</sup>*Inorganic Chemistry & Catalysis, Debye Institute for Nanomaterials Science,  
Utrecht University, Universiteitsweg 99, 3584 CG, Utrecht, The Netherlands*

<sup>2</sup>*Institute for Solid State Physics, TU Wien, 1040 Vienna, Austria*

<sup>3</sup>*Institute of Physics, Czech Academy of Sciences, Na Slovance 2, 182 21 Praha 8, Czechia*

<sup>4</sup>*Imperial College London, Department of Materials, Exhibition Road, London SW7 2AZ, UK*

<sup>5</sup>*Diamond Light Source, Didcot, OX11 0DE, UK*

<sup>6</sup>*Canadian Light Source, Saskatoon, SK S7N 2V3, Canada*

<sup>7</sup>*Synchrotron SOLEIL, l'Orme des Merisiers, Saint-Aubin, BP 48, F-91192 Gif-sur-Yvette Cedex, France*

<sup>8</sup>*Sorbonne Université, CNRS, Laboratoire de Chimie Physique-Matière et Rayonnement, LCPMR, F-75005 Paris, France*

(Dated: May 2, 2022)

We study 1s and 2p hard x-ray photoemission spectra (XPS) in a series of late transition metal oxides: Fe<sub>2</sub>O<sub>3</sub> (3d<sup>5</sup>), FeTiO<sub>3</sub> (3d<sup>6</sup>), CoO (3d<sup>7</sup>) and NiO (3d<sup>8</sup>). The experimental spectra are analyzed with two theoretical approaches: the MO<sub>6</sub> cluster model and the local density approximation (LDA) + dynamical mean-field theory (DMFT). Owing to the absence of the core-valence multiplets and spin-orbit coupling, 1s XPS is found to be a sensitive probe of chemical bonding and nonlocal charge-transfer screening, providing complementary information to 2p XPS. The 1s XPS spectra are used to assess the accuracy of the *ab-initio* LDA+DMFT approach, developed recently to study the material-specific charge-transfer effects in core-level XPS.

## I. INTRODUCTION

Transition metal oxides are an important class of functional materials, showing a variety of fascinating phenomena, such as giant magnetoresistance and spontaneous ordering of spin, charge or orbital degrees of freedom [1, 2]. Thanks to the progress in using the hard x-ray sources in the last decade core-level x-ray photoemission spectroscopy (XPS) [3–5] has become a powerful tool to study the electronic properties of transition metal oxides [1, 6]. Electronic response to the local charged perturbation (core hole) gives rise to specific features in the 2p XPS spectra due to the charge-transfer screening from distant atoms, traditionally called nonlocal screening [7–9], in addition to local screening from the neighboring ligands. The nonlocal screening features are sensitive to various aspects of physics in transition-metal oxides including magnetic and orbital order, and metal-insulator transition [8–17].

In 2p XPS, the charge-transfer features are buried in complex spectra reflecting the 2p-3d core-valence multiplets and spin-orbit coupling in the 2p shell. These effects are absent in the 1s XPS spectra. In practice, little additional effort is required to measure 1s XPS together with valence or other core-level spectra. Despite the large life-time broadening, the absence of the core-valence multiplets and spin-orbit coupling allows 1s XPS to be used: (1) to identify charge-transfer satellites at higher binding energies, which enables an accurate estimation of material-specific parameters [18, 19], (2) to distinguish local and nonlocal screening features. We note that in principle there is a 1s3d exchange interaction but the interaction strength is only a few meV and this effect is not visible in the spectral shape.

The cluster model including the excited transition-metal ion and neighboring ligands has been widely employed in core-level XPS studies [6, 20]. The adjustable parameters of the cluster model can be to a large extent eliminated by *ab-initio* low-energy Hamiltonians in the basis of the localized Wannier orbitals [21]. To account for nonlocal screening missing in the cluster model, an *ab-initio* method based on local-density approximation (LDA) + dynamical mean-field theory (DMFT) was introduced recently [9, 22], see also Ref. [23] in a similar direction. In this approach, the Anderson impurity model with the DMFT hybridization function  $V(\varepsilon)$  is extended to include explicitly the core orbitals and their interaction with transition metal 3d orbitals.

In this paper, we present a combined experimental and theoretical study of 1s and 2p XPS spectra in selected late transition-metal oxides: Fe<sub>2</sub>O<sub>3</sub>, FeTiO<sub>3</sub>, CoO and NiO. By comparison of the cluster-model and LDA+DMFT calculations, we distinguish the local- and nonlocal screening contributions in the 1s and 2p spectra. Asymmetric shape of the main 1s XPS line is found to be a fingerprint of nonlocal screening in the studied compounds. The accuracy of the *ab-initio* material-specific parameters is examined by comparing to the present 1s XPS data.

## II. EXPERIMENTAL DETAILS

The 1s XPS and 2p XPS spectra of  $\alpha$ -Fe<sub>2</sub>O<sub>3</sub> single crystal were measured at ID16 beamline of ESRF. For this sample, photon energy of 10 keV and 7.7 keV were used to measure the Fe 1s and the Fe 2p photoemission spectra, respectively. The overall energy resolution at

10 keV is 0.48 eV and at 7.7 keV is 0.42 eV.

The 1s XPS (photon energy of 9 keV) and 2p XPS (photon energy of 3 keV) spectra of the single crystal CoO sample were measured at SXRMB beamline of the Canadian Light Source (CLS), with a resolving power of  $(E/\Delta E)$  of  $\sim 10^4$ .

The Ni 1s XPS of NiO was measured at the HIKE station of the KMC-1 beamline at BESSY. The incident x-ray beam of  $\sim 8.9$  keV was used while the Si(422) crystal provided the resolution of  $\sim 0.5$  eV. The NiO thin film was grown on a Ag substrate, and capped by 3 nm of MgO to avoid the charging effects [24]. The NiO was grown with the NiO (001) direction parallel to Ag (001).

The 1s XPS and 2p XPS spectra of FeTiO<sub>3</sub> (Fe<sup>2+</sup>) powders were measured at I09 beamline of Diamond light source. FeTiO<sub>3</sub> (99.8%) powders were purchased from Alfa Aesar. For the 1s XPS and 2p XPS measurements, photon energies of 6 keV and 12 keV were used, respectively. Resolution at 6 keV is 250 meV, while resolution at 12 keV is 300 meV. All the measurements were collected at room temperature.

### III. COMPUTATIONAL METHOD

#### A. Theoretical Methods

The 1s and 2p XPS spectra are analyzed by the cluster model and the LDA+DMFT approach. In both cases, we start with a standard LDA calculation using the Wien2K package [25] for the experimental crystal structure. Then the tight-binding representation of the transition metal 3d and O 2p bands is constructed using the Wannier90 package [26] and Wien2wannier interface [27]. The  $d$ - $p$  model is augmented with the electron-electron interaction within the transition metal 3d shell, leading to the lattice Hamiltonian

$$H = \sum_{\mathbf{k}} (d_{\mathbf{k}}^\dagger \ p_{\mathbf{k}}^\dagger) \begin{pmatrix} h_{\mathbf{k}}^{dd} - \mu_{dc} & h_{\mathbf{k}}^{dp} \\ h_{\mathbf{k}}^{pd} & h_{\mathbf{k}}^{pp} \end{pmatrix} \begin{pmatrix} d_{\mathbf{k}} \\ p_{\mathbf{k}} \end{pmatrix} + \sum_i W_i^{dd}. \quad (1)$$

Here,  $d_{\mathbf{k}}$  ( $p_{\mathbf{k}}$ ) is an operator-valued vector whose elements are Fourier transforms of  $d_{\alpha i}$  ( $p_{\gamma i}$ ), that annihilates the transition metal 3d (O 2p) electron in the orbital  $\alpha$  ( $\gamma$ ) in the  $i^{\text{th}}$  unit cell.  $W_i^{dd}$  is the on-site Coulomb interaction acting on the transition metal  $d$  shell. The double-counting term  $\mu_{dc}$ , which corrects for the  $d$ - $d$  interaction present in the LDA step, renormalizes the  $p$ - $d$  splitting, thus relates to the charge transfer energy  $\Delta$  [9, 22, 28]. The relation of  $\Delta$  and  $\mu_{dc}$  can be given as,  $\Delta = \varepsilon_d - \mu_{dc} + n \times U_{dd} - \varepsilon_p$ , where  $\varepsilon_d$  ( $\varepsilon_p$ ) is the average energy of transition metal 3d (O 2p) states and  $U_{dd}$  is the value of the (configuration-averaged) Coulomb interaction. Here,  $\Delta$  is defined for a formal valence, as employed in conventional spectroscopy studies [6, 20]. The calculation temperature is set to  $T = 300$  K in the present study. We note that, in NiO, CoO and Fe<sub>2</sub>O<sub>3</sub>, the unit cell is enlarged to simulate the antiferromagnetic ordering ob-

served experimentally below 300 K [29]. In FeTiO<sub>3</sub>, the unit cell contains Ti and Fe atoms. The Hamiltonian of the cluster model consists of terms including single transition metal ion and its neighboring ligands in Eq. (1).

In the LDA+DMFT approach, we first solve the lattice model of Eq. (1) within DMFT [30, 31]. In the present study, the strong-coupling continuous-time quantum Monte Carlo method [32–35] with density-density approximation to the on-site interaction was used to compute the self-energy of the auxiliary Anderson impurity model. Upon reaching the LDA+DMFT self-consistency, the self-energy is analytically continued with the maximum entropy method [36, 37] in order to obtain the hybridization function  $V(\varepsilon)$  in the real-frequency domain. Next, we augment the Anderson impurity model with the core orbitals (1s or 2p), add the core-valence interaction and drop the density-density interaction to  $dd$  interaction.

The core-level XPS spectrum is calculated with the truncated configuration interaction method [9]. The XPS spectral function for the binding energy  $E_B$  is given by [6, 9]

$$F_{\text{XPS}}^{(n)}(E_B) = -\frac{1}{\pi} \sum_n \langle n | T^\dagger \frac{1}{E_B + E_n - H_{\text{model}}} T | n \rangle,$$

where  $E_n$  is the eigen energy of the  $n$ -th excited states  $|n\rangle$  in the initial state. The temperature effect is taken into account with the Boltzmann factor at  $T = 300$  K. The operator  $T$  creates a 1s or 2p core hole at the impurity transition-metal site. Here  $H_{\text{model}}$  is the model Hamiltonian, i.e. the Hamiltonian of the cluster model or the Anderson impurity model with the DMFT hybridization function.

In the cluster-model calculation, we employ the CTM4XAS program [38], and adopt a standard three configuration scheme. The computational details in the LDA+DMFT method can be found in Refs. [9, 22].

#### B. Computational Parameters

The following computational parameters are used both in the cluster model and LDA+DMFT method: the Coulomb interaction of the 3d electrons  $U_{dd}$ ; the core-valence Coulomb interactions  $U_{sd}$  ( $U_{pd}$ ) in the 1s (2p) XPS; Slater integrals representing the multipole part of the Coulomb interaction; one-particle hopping parameters; crystal-field splitting; and charge-transfer energy  $\Delta$ . The  $U_{dd}$  value is fixed by consulting with DFT-based estimations or previous XPS studies, as given in Table I. The core-hole potential  $U_{sd}$  ( $U_{pd}$ ) is fixed by fitting the experimental core-level spectra. The spin-orbit coupling in the 2p and 3d shell, and the Slater integrals  $F_k$ ,  $G_k$  of 2p-3d and 1s-3d core-valence Coulomb interaction are calculated with an atomic Hartree-Fock code. The  $F_k$  and  $G_k$  values are scaled down to 80% of the Hartree-Fock values to simulate the effect of intra-atomic configuration

	Fe <sub>2</sub> O <sub>3</sub> Fe <sup>3+</sup> ( <i>d</i> <sup>5</sup> )	FeTiO <sub>3</sub> Fe <sup>2+</sup> ( <i>d</i> <sup>6</sup> )	CoO Co <sup>2+</sup> ( <i>d</i> <sup>7</sup> )	NiO Ni <sup>2+</sup> ( <i>d</i> <sup>8</sup> )
10 <i>Dq</i>	0.5	0.25	0.25	0.45
Δ	3.7	3.5	4.1	4.4
<i>U</i> <sub><i>s</i><i>d</i></sub> ( <i>U</i> <sub><i>p</i><i>d</i></sub> )	8.4	8.0	8.6	7.8
<i>U</i> <sub><i>dd</i></sub>	6.4	6.4	6.8	6.5
<i>V</i> <sub><i>T</i><sub>2<i>g</i></sub></sub>	1.3	1.3	1.2	1.2
<i>V</i> <sub><i>E</i><sub>g</sub></sub>	2.5	2.1	2.0	2.1

TABLE I. Summary of the parameter values in the present study: crystal-field splitting between *E<sub>g</sub>* and *T<sub>2g</sub>* states (10*Dq*), charge-transfer energy (Δ), core-hole potential for 1*s* (*U<sub>sd</sub>*) and 2*p* (*U<sub>pd</sub>*) XPS, 3*d* Coulomb interaction (*U<sub>dd</sub>*), hopping amplitude of the nearest-neighboring ligand states and transition metal *E<sub>g</sub>* (*V<sub>Eg</sub>*) and *T<sub>2g</sub>* (*V<sub>T2g</sub>*) state. In Fe<sub>2</sub>O<sub>3</sub> and FeTiO<sub>3</sub>, the triply-degenerate *T<sub>2g</sub>* states split into double-degenerate *E<sub>gπ</sub>* states and single *A<sub>1g</sub>* state. The values of the *T<sub>2g</sub>* state in the table are obtained by averaging over the ones of the *E<sub>gπ</sub>* and *A<sub>1g</sub>* states. In actual calculation, the splitting of the *E<sub>gπ</sub>* and *A<sub>1g</sub>* states is taken into account explicitly. All values are in eV.

interaction from higher basis configurations, which is a successful empirical treatment [39–43]. The one-particle hopping and the crystal-field parameters are computed from the LDA bands. The double-counting correction  $\mu_{dc}$  in LDA+DMFT is treated as an adjustable parameter and fixed by comparison to the valence photoemission spectra [9]. For FeTiO<sub>3</sub>,  $\mu_{dc}$  is determined to reproduce the experimental gap ( $\sim 2.5$  eV) [44] since valence photoemission data are not reported so far. The computed XPS intensities are broadened using the Gaussian and Lorentzian function to simulate the instrumental resolution and the finite core-hole life time.

### C. Hybridization Function

The hybridization function  $V(\varepsilon)$  describes electron hopping between the 3*d* orbitals on the x-ray excited transition-metal site and the rest of the crystal. In LDA+DMFT, the  $V(\varepsilon)$  for orbital  $\gamma$  and spin  $\sigma$  is obtained from [45],

$$V_{\gamma\sigma}^2(\varepsilon) = -\frac{1}{\pi} \text{Im} \langle d_{\gamma\sigma} | (\varepsilon - h^0 - \Sigma(\varepsilon) - G^{-1}(\varepsilon)) | d_{\gamma\sigma} \rangle, \quad (2)$$

where  $\Sigma(\varepsilon)$  and  $h^0$  are the local self-energy and the one-body part of the on-site Hamiltonian, respectively [9, 30, 31]. The local Green's function  $G(\varepsilon)$  is computed by averaging the lattice Green's function over the Brillouin zone. In a non-interacting host, the hybridization function  $V(\varepsilon)$  can be decomposed to the distance-shell contributions,

$$V_{\gamma\sigma}^2(\varepsilon) = -\frac{1}{\pi} \text{Im} \langle d_{\gamma\sigma} | V_{hi}^\dagger \frac{1}{\varepsilon - h_{\text{host}}} V_{hi} | d_{\gamma\sigma} \rangle, \quad (3)$$

where  $V_{hi}$  represents the hopping terms between the transition metal 3*d* orbitals on the impurity site and *i*-th site

of the crystal. Here,  $h_{\text{host}}$  is the host Hamiltonian which contains all terms in Eq. (1) except for ones including the x-ray excited transition-metal site. We use Eq. (3) to compute  $V(\varepsilon)$  of the cluster model as well as the (non-interacting) finite-size clusters to demonstrate hopping-distance dependence of  $V(\varepsilon)$  structure. Note, that similar expression for  $V_{\gamma\sigma}^2(\varepsilon)$  holds also for an interacting host (with an additional self-energy in the denominator), however, decomposition to different hopping cut-offs is not strictly defined since all hoppings are implicitly present in the self-energy.

## IV. RESULTS

### A. NiO

We start with NiO, a prototype Mott insulator with a large charge gap ( $\sim 4$  eV). Figure 1 shows Ni 1*s* and 2*p* XPS spectra of NiO. The Ni 2*p* XPS spectrum is composed of 2*p*<sub>3/2</sub> (868~853 eV) and 2*p*<sub>1/2</sub> (880~870 eV) components. The 2*p*<sub>3/2</sub> (2*p*<sub>1/2</sub>) main line around 854 eV (873 eV) corresponds to  $\underline{c}d^9\underline{v}$  configuration, where  $\underline{c}$  and  $\underline{v}$  denote 2*p* core-hole and hole in the valence band, respectively. The 2*p*<sub>3/2</sub> (2*p*<sub>1/2</sub>) charge-transfer satellite around 861 eV (878 eV) has a mixed character of  $\underline{c}d^8$  and  $\underline{c}d^{10}\underline{v}^2$  configurations. A double-peak feature is observed in the 2*p*<sub>3/2</sub> main line. The lower (higher) binding-energy *E<sub>B</sub>* side of the double peaks is due to the nonlocal (local) screening in the final states [9, 11, 15]. The LDA+DMFT result qualitatively reproduces the Ni 2*p* XPS data including the double-peak that is missing in the cluster-model result. In addition, the charge transfer satellite shows a noticeable difference in the the cluster and LDA+DMFT results, indicating the nonlocal screening affects not only the main line but also the satellite with a higher binding energy. This is because the charge transfer satellite has a contribution of the  $\underline{c}d^{10}\underline{v}^2$  configuration, the so-called over-screened states, in which the nonlocal screening takes part. The spin-orbit coupling in the Ni 2*p* core level is large ( $\sim 11$  eV). Thus the Ni 2*p*<sub>3/2</sub> and 2*p*<sub>1/2</sub> components have no overlap.

The Ni 1*s* XPS, see Fig. 1a, is free from spin-orbit coupling in the core level. Besides the main line around 8298 eV, the charge-transfer satellite is clearly observable around 8305 eV. A double peak is discernible in the main line despite larger core-hole broadening. The similarity to the 2*p*<sub>3/2</sub> main line and its presence/absence in the LDA+DMFT/cluster-model spectra suggests its nonlocal screening origin. The splittings of the main line and the charge-transfer satellite in the Ni 1*s* and 2*p* spectra are almost identical to each other ( $\sim 6$  eV), indicating the values of the core-hole potential *U<sub>sd</sub>* and *U<sub>pd</sub>* are comparable. Indeed, the LDA+DMFT calculation with *U<sub>sd</sub>* = *U<sub>pd</sub>* = 7.8 eV well reproduces the splitting of the main and charge transfer satellite in both the 1*s* and 2*p* XPS spectra.

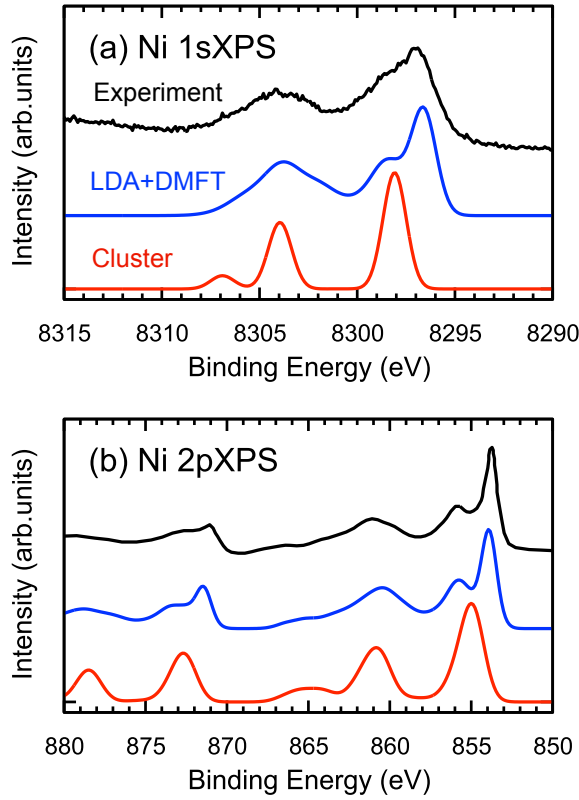


FIG. 1. (Color online) Experimental Ni 1s and 2p XPS spectra of NiO (black) are compared with LDA+DMFT in the antiferromagnetic phase (blue) and cluster-model (red) calculations. The Gaussian spectral broadening of 0.9 (0.5) eV (HWHM) is taken into account in the calculated 1s (2p) spectra. The experimental Ni 2p XPS data is taken from Ref. [11].

## B. CoO

CoO is a typical transition-metal oxide with a large charge gap  $\sim 3.6$  eV. Figure 2 shows Co 1s and 2p XPS spectra of CoO, together with the calculated spectra by the cluster model and LDA+DMFT. The Co  $2p_{3/2}$  and  $2p_{1/2}$  components are located in 794-778 eV and 807-795 eV range, respectively. The Co  $2p_{3/2}$  main line (satellite) has an energy of 780 eV (787 eV). The Co  $2p_{3/2}$  main line is rather broad in a clear contrast to the double-peak feature in the Ni  $2p_{3/2}$  main line. The LDA+DMFT result well reproduces the broad shape of the main line as well as of the charge transfer satellite, compared to the cluster-model result. The difference between the LDA+DMFT and cluster-model results suggests that the nonlocal screening from Co 3d bands plays a role in the formation of the broad asymmetric main line [9]. However, the Co  $2p_{3/2}$  main line in the cluster-model result has inner features due to rich 2p-3d core-valence multiplets in the  $\underline{cd}^8\underline{v}^1$  configuration. Thus a theoretical simulation is required to disentangle the local screening and nonlocal screening contributions in the Co 2p spectra [9]. As in the Ni 2p XPS, the nonlocal screen-

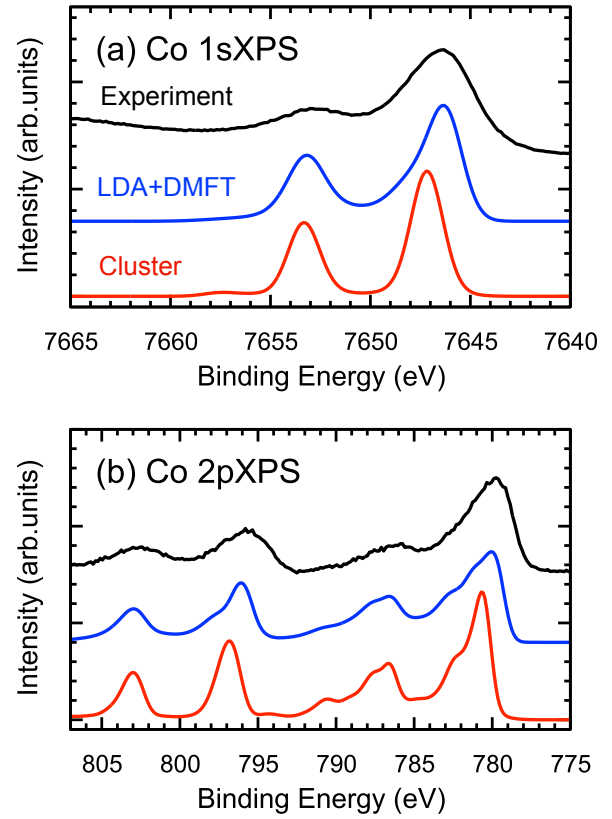


FIG. 2. (Color online) Experimental Co 1s and 2p XPS spectra of CoO (black) are compared with LDA+DMFT (blue) and cluster-model (red) calculations. The Gaussian spectral broadening of 1.1 (0.5) eV (HWHM) is taken into account in the calculated 1s (2p) spectra.

ing in the over-screened configuration  $\underline{cd}^9\underline{v}^2$  affects the shape of a higher  $E_B$  part of the charge-transfer satellite ( $\sim 790$  eV).

The Co 1s XPS, see Fig. 2a, shows the main line ( $\sim 7647$  eV) and the satellite ( $\sim 7653$  eV). The splitting of the main line and the charge-transfer satellite in the 1s and 2p spectra is almost identical ( $\sim 6$  eV). The main line has an asymmetric shape with a shoulder on the higher  $E_B$  side. Because of the absence of the core-valence multiplets in Co 1s spectra, the Co 1s main line is expected to be a single peak. Indeed, the cluster-model calculation yields a symmetric main line. On the other hand, the LDA+DMFT spectrum contains asymmetric main line, suggesting the nonlocal screening is the origin of the asymmetry of the main line.

## C. Fe<sub>2</sub>O<sub>3</sub>

$\alpha$ -Fe<sub>2</sub>O<sub>3</sub> is an insulating Fe<sup>3+</sup> oxide with corundum structure and antiferromagnetic ordering below  $T_N \sim 950$  K. Figure 3 shows Fe 1s and 2p XPS spectra, together with the calculated spectra by LDA+DMFT and cluster

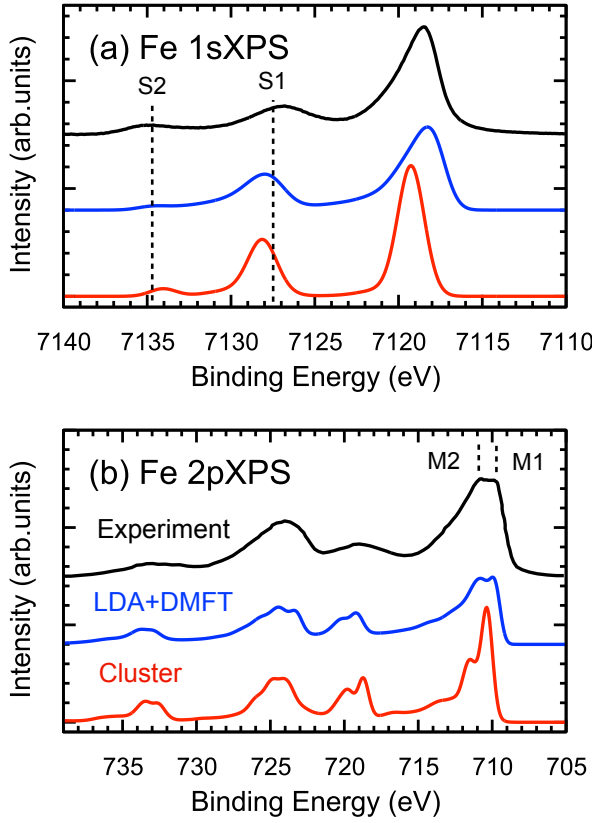


FIG. 3. (Color online) Experimental Fe 1s and 2p XPS spectra of Fe<sub>2</sub>O<sub>3</sub> (black) are compared with LDA+DMFT (blue) and cluster-model (red) calculations. The spectral broadening using a Gaussian of 0.9 (0.4) eV width (HWHM) is taken into account in the calculated 1s (2p) spectra. The experimental data of Fe 2p XPS is taken from Ref. [18]. In the 1s spectra, the first and second satellites are labeled as S1 and S2 in Fig. 3a, respectively.

model. The Fe 1s spectrum shows three peaks: main line ( $\sim 7118.5$  eV), the first satellite (S1 :  $\sim 7128$  eV) and the second satellite (S2 :  $\sim 7135$  eV). The energy splittings of the main line and satellites are rather large ( $\sim 9.5$  eV for S1 and  $\sim 17$  eV for S2) compared to those in NiO and CoO ( $\sim 6$  eV). The large splitting in Fe<sub>2</sub>O<sub>3</sub> can be explained by the value of the effective hybridization  $V_{\text{eff}}$  [6, 46, 47],

$$V_{\text{eff}} = \sqrt{(4 - N_{E_g}) \times V_{E_g}^2 + (6 - N_{T_{2g}}) \times V_{T_{2g}}^2},$$

where  $N_{E_g}$  ( $N_{T_{2g}}$ ) and  $V_{E_g}$  ( $V_{T_{2g}}$ ) are the occupation of the  $E_g$  ( $T_{2g}$ ) states and the (bare) hybridization intensity between ligand and the  $E_g$  ( $T_{2g}$ ) orbitals [48]. The  $V_{\text{eff}}$  values in NiO, CoO and Fe<sub>2</sub>O<sub>3</sub>, computed for high-spin ground state in formal valence, are 2.97, 3.24, and 4.19 eV, respectively. Thus the different configurations ( $d^n$ ,  $d^{n+1}\underline{L}$ ,  $d^{n+2}\underline{L}^2$ , here  $\underline{L}$  denotes a hole in nearest neighboring ligands) are split more in Fe<sub>2</sub>O<sub>3</sub> as compared to NiO and CoO, yielding the large separations of the main line and satellites in Fe 1s XPS. Thus

in Fe and earlier transition-metal oxides [46, 47, 49], the hybridization strength between transition metal 3d and surrounding atoms can be estimated accurately by the satellite positions since the large  $V_{\text{eff}}$  magnifies its bare value. Both the LDA+DMFT and the cluster-model calculations reproduce the positions of the satellites reasonably well, reflecting the accuracy of hopping parameters obtained from the LDA calculation. However, in the Fe 2p spectrum, Fig. 3b, the second satellite S2 is not visible due to its overlap with the main line of the Fe 2p<sub>1/2</sub> component ( $\sim 725$  eV). Thus, thanks to absence of spin-orbit coupling, 1s XPS complements the 2p XPS information about bonding.

The Fe 2p<sub>3/2</sub> main line shows a double-peak shape, marked as M1 and M2 in the figure, that is well reproduced in the LDA+DMFT result. The difference in the LDA+DMFT and cluster-model results is attributed to the contribution of the nonlocal screening, the M2 intensity is enhanced relative to the M1 one. However, as seen in the cluster-model spectrum, Fig. 3b, the main line has a rich fine structure also due to the core-valence Coulomb multiplets, which makes determination of the nonlocal screening contribution a difficult task. On the contrary, the asymmetry of the Fe 1s XPS main line, observed in the experiment, Fig. 3a, is solely due to nonlocal screening. As in CoO, the 1s main line of the cluster model consists of a single peak due to the absence of the core-valence multiplets, while that of the LDA+DMFT shows a clear asymmetry. Thus the shape of the 1s XPS main line provides an unambiguous signature of the nonlocal screening, while it is hidden in the complex structure of 2p XPS.

#### D. FeTiO<sub>3</sub>

Figure 4 shows the experimental Fe 1s and 2p XPS spectra. In the Fe 1s spectrum, we observe a main line ( $\sim 7090$  eV) and a CT satellite (S1 :  $\sim 7097$  eV). The energy splitting between the CT satellite (S1) and main line is 7 eV which is about 2.5 eV smaller compared to that in Fe<sub>2</sub>O<sub>3</sub>, see Fig. 3a. As found in Table. I, the hopping amplitude between Fe and nearest-neighboring oxygen as well as other parameters does not differ so much in the two compounds. The large difference in the main-line – CT-satellite splitting comes from the value of the  $V_{\text{eff}}$ , 4.19 eV for Fe<sub>2</sub>O<sub>3</sub> and 3.49 eV for FeTiO<sub>3</sub>. The  $V_{\text{eff}}$  value in the divalent Fe system ( $d^6$ ) is smaller than that in the trivalent Fe system ( $d^5$ ) due to an additional electron in the  $T_{2g}$  orbital in the high-spin ground state, resulting in the observed smaller main-satellite splitting in FeTiO<sub>3</sub>. In FeTiO<sub>3</sub>, a higher- $E_B$  CT satellite (S2) is rather weak and not observed in the present data, which is due to little contribution of the  $|d^8v^2\rangle$  configuration to the ground state. The position of S1 and the absence of S2 are well reproduced in the LDA+DMFT calculation.

We expect that the nonlocal screening plays a minor role in FeTiO<sub>3</sub> compared to Fe<sub>2</sub>O<sub>3</sub> since Ti ions, formally

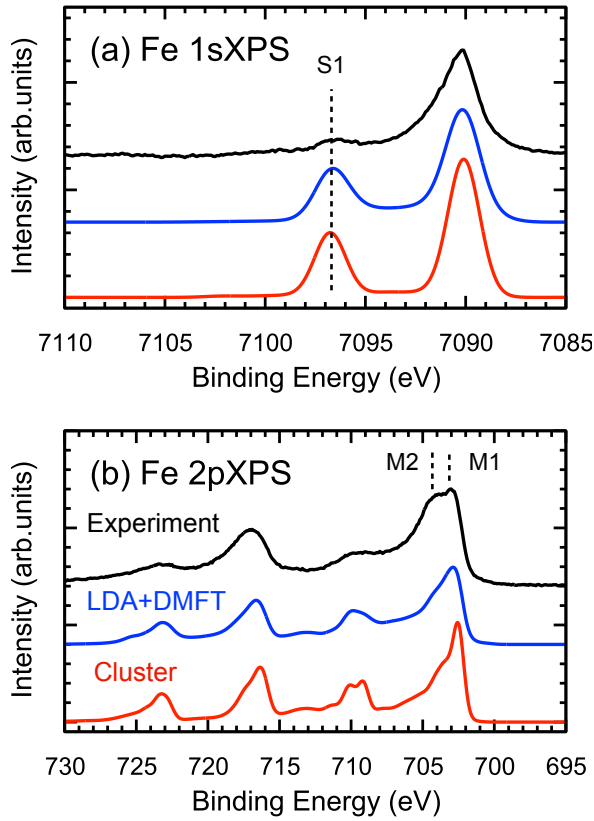


FIG. 4. (Color online) Experimental Fe 1s and 2p XPS spectra of FeTiO<sub>3</sub> (black) are compared with LDA+DMFT (blue) and cluster-model (red) calculations. The spectral broadening using a Gaussian of 1.1 (0.4) eV width (HWHM) is taken into account in the calculated 1s (2p) spectra.

tetravalent  $d^0$  configuration, cannot provide electrons to screen the x-ray excited Fe ion. Simulation of the Fe 2p XPS of Fe<sub>2</sub>O<sub>3</sub>, Fig. 3b, revealed that nonlocal screening amplifies the intensity of M2 relative to M1. This is confirmed by comparing the experimental data of Fe<sub>2</sub>O<sub>3</sub> and FeTiO<sub>3</sub>. In FeTiO<sub>3</sub>, Fig. 4b with weaker nonlocal screening, a smaller ratio of M2 to M1 intensities than in Fe<sub>2</sub>O<sub>3</sub> is observed. Indeed, the LDA+DMFT spectra of FeTiO<sub>3</sub> do not differ much from the cluster-model calculation, though the relative intensity of M1 and M2 is still noticeably modified by NLS. The main line of Fe 1s XPS in FeTiO<sub>3</sub> is rather sharp compared to that in Fe<sub>2</sub>O<sub>3</sub>, see the fittings in the Appendix, indicating less nonlocal screening contribution.

## V. DISCUSSION

All spectral features in the studied compounds are well reproduced by the LDA+DMFT approach. This is not so for the cluster model and the comparison of the two models provides information about the nonlocal screening effects. Despite rather large life-time broadening of the 1s spectra compared with the 2p counterparts, the

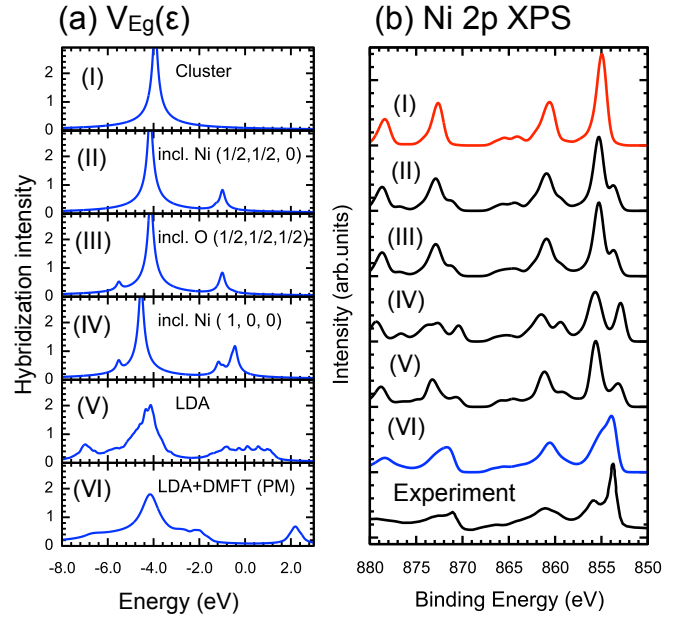


FIG. 5. (Color online) (a) Hybridization intensities for the  $E_g$  state in NiO. From top to bottom, the long-distance hoppings including the atom denoted in the bracket are taken into account.  $V(\epsilon)$  in panels (I)–(IV) and (V) are computed in the non-interacting finite-size clusters and infinite lattice, respectively. The  $V(\epsilon)$  obtained in the LDA+DMFT calculation for the paramagnetic phase is shown in panel (VI), for comparison. The  $V(\epsilon)$  for the antiferromagnetic phase is found in Ref. [9]. (b) Ni 2p XPS calculated by the Anderson impurity model with the hybridization intensities in Fig. (a).

charge-transfer satellites are clearly visible for the studied compounds. This holds also for charge-transfer satellites at higher binding energies, which are not obscured by the overlap of spin-orbit split edges as in the 2p spectra. The 1s charge-transfer satellites, usually well pronounced in the spectra of correlated insulators, thus provide information about covalent bonding in these compounds. Absence of the core-valence multiplets in 1s XPS directly reveals the effect of nonlocal screening reflected in the asymmetry of the 1s main line.

The shape of the 1s XPS spectra has implications for the interpretation of 1s ( $K$ -edge) x-ray absorption spectroscopy (XAS). In  $K$ -edge XAS, the electron excited from the 1s core-level to the broad 4p band is not bound to the excited transition-metal atom. The fact the 1s XPS spectra have multiple peaks implies that one X-ray photon energy creates a series of electrons with different kinetic energies. This is in contrast to the usual way to calculate  $K$ -edge XAS, i.e. it is assumed that the X-ray photon creates a single electron kinetic energy. To take the spectral shape of the 1s XPS spectra into account, the  $K$ -edge XAS spectra must be viewed as a convolution of the empty 4p density of state (as calculated from for example multiple scattering) and the 1s XPS spectrum. In other words, the detailed understanding of the  $K$ -edge XAS spectral shape requires the inclusion of



many-body response to the core-hole potential as measured with the  $1s$  XPS spectral shape, where we note that this approach is similar in concept to the charge-transfer satellite method as applied earlier [50–52]. If the  $1s$  XPS spectral shape can be described by a single peak, the related  $K$ -edge XAS can be described from the multiple scattering of a single electron energy [53]. As shown here, charge-transfer satellites present a sizable contribution to the  $1s$  XPS of late transition-metal oxides. Therefore a simultaneous analysis  $1s$  XPS and  $1s$  XAS is desirable for the detailed understanding of the  $1s$  XAS spectral shape.

Finally, we discuss the theoretical description of nonlocal screening core-level XPS. In contrast to the real-space approach of the multi-site cluster model [7] LDA+DMFT includes both local-screening and nonlocal-screening effects in the hybridization function  $V(\varepsilon)$  of the Anderson impurity model. To see the connection between this description and the real-space one, Fig. 5a shows the distance dependence of the hybridization intensity  $V(\varepsilon)$  in NiO. Starting from a single peak in the  $V(\varepsilon)$  of the cluster model, which corresponds to the hybridization with nearest-neighboring oxygen atoms,  $V(\varepsilon)$  acquires a band character by taking more distant atoms into account. We note that the truncated  $V(\varepsilon)$  in panels (I)-(IV) and (V) is computed in non-interacting finite-size clusters and infinite lattice, respectively. The intensities around  $-2 \sim 2$  eV corresponds to the hybridization with Ni  $3d$  bands. These intensities are rather weak compared to those arising from O  $2p$  bands ( $\sim -4$  eV) due to a smaller amplitude of direct metal-metal hopping as well as indirect hopping, e.g., via a metal-ligand-metal path. The electronic correlation represented by DMFT self-energy modifies the  $V(\varepsilon)$  dramatically and a gap opens at the Fermi energy. Figure 5b shows the calculated  $2p$  XPS spectra by the Anderson impurity model with the truncated hybridization intensities  $V(\varepsilon)$ . By taking surrounding Ni ions into account, a new peak develops in the low-binding-energy side of the main line. However we find a qualitative difference in the main-line shape between the experimental data and the spectra in (I)-(V). The LDA+DMFT result in the paramagnetic phase, see (VI), shows double peaks in the main line although their splitting of is rather narrow. The LDA+DMFT result in the antiferromagnetic phase, see Fig. 1b, reproduces the double-peak feature qualitatively. The  $V(\varepsilon)$  in LDA, in principle, includes hybridization with all valence states in the non-interacting lattice, indicating the importance to include the correlated Ni  $3d$  band and the magnetic ordering properly to describe the XPS spectra.

## VI. CONCLUSIONS

We have studied both experimentally and theoretically the  $1s$  and  $2p$  hard x-ray photoemission spectra (XPS) in a series of late transition metal oxides:  $\text{Fe}_2\text{O}_3$ ,  $\text{FeTiO}_3$ ,  $\text{CoO}$  and  $\text{NiO}$ . Despite the large core-hole life-time broad-

ening, the  $1s$  XPS benefits from the absence of core-valence multiplets and spin-orbit coupling effects in the spectra, which allows observation of high-energy satellites as well as the main-line asymmetry. These  $1s$  XPS features can be interpreted in terms of material specific metal-ligand covalency (satellites) and nonlocal screening (main-line asymmetry). The  $1p$  XPS is thus complementary to  $2p$  XPS that has more complex spectra. Using LDA+DMFT approach we were able to reproduce the  $1s$  and  $2p$  XPS spectra of the studied materials, while the deviations from the cluster model allowed us to quantify the role of nonlocal screening. Based on the present  $1s$  XPS results, we have pointed out the importance of the  $1s$  XPS to interpret the  $1s$  ( $K$ -edge) x-ray absorption spectra.

## ACKNOWLEDGMENTS

The authors thank T. Uozumi, P. S. Miedema, A. Sotnikov and J. Fernández Afonso for fruitful discussions, and Ties Haarman for providing the fitting code. We thank R.-P. Wang for supporting the fitting analysis. Diamond Light Source, Canadian Light Source, ESRF and BESSY II are acknowledged for the allocation of synchrotron radiation beamtimes at the I09, SXRMB, ID16, and KMC-1 beamlines, respectively. A. H., M.W. and J. K. are supported by the European Research Council (ERC) under the European Union’s Horizon 2020 research and innovation programme (grant agreement No. 646807-EXMAG). M. G. and F. M. F. de G. are supported by an European Research Council (ERC) grant XRAYonACTIVE (No. 340279). AR acknowledges the support from Imperial College London for her Imperial College Research Fellowship. The computational calculations were performed at the Vienna Scientific Cluster (VSC).

## APPENDIX: FITTING ANALYSIS OF THE $1s$ XPS DATA

Figure 6 shows the fitting analysis of the  $1s$  XPS experimental data of  $\text{CoO}$ ,  $\text{Fe}_2\text{O}_3$ , and  $\text{FeTiO}_3$ . The main line is fitted using two Pseudo-Voigt functions composed of 20% Lorentzian and 80% of Gaussian. Considering the present experimental energy resolution and typical life-time of the  $1s$  core hole, the width (HWHM) of the Lorentzian  $\Gamma_L$  and Gaussian  $\Gamma_G$  is set to  $(\Gamma_L, \Gamma_G) = (0.28, 1.12)$ ,  $(0.29, 0.91)$ , and  $(0.20, 0.80)$  in the unit of eV for  $\text{CoO}$ ,  $\text{Fe}_2\text{O}_3$ , and  $\text{FeTiO}_3$ , respectively. For the satellites, the widths of the Pseudo-Voigt functions are relaxed to reproduce the experimental data. The background in the experimental data is subtracted prior to the fitting analysis using the Shirley method [54]. This fitting analysis confirms the asymmetry of the  $1s$  main line in  $\text{CoO}$ ,  $\text{Fe}_2\text{O}_3$ , and  $\text{FeTiO}_3$ . The intensity ratio of the low-energy peak ( $I_1$ ) to the high-energy peak ( $I_2$ )

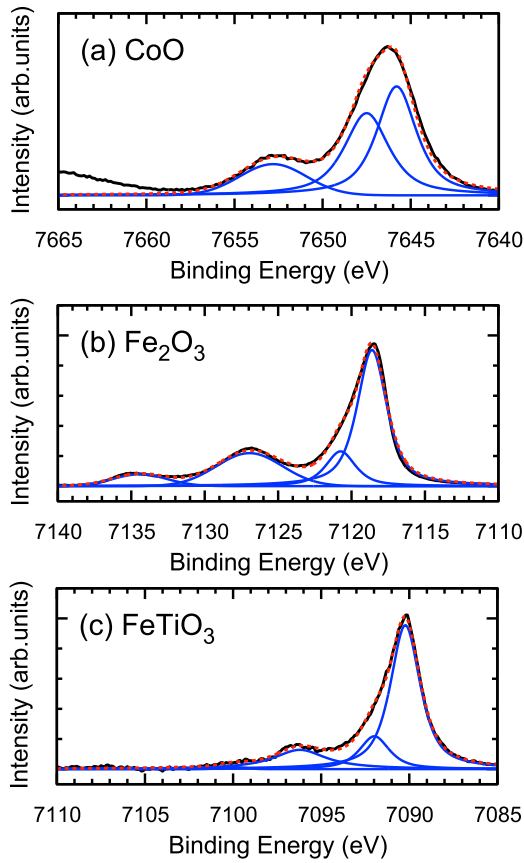


FIG. 6. (Colour online) Fitting analysis of the 1s XPS experimental data for (a) CoO, (b) Fe<sub>2</sub>O<sub>3</sub>, and (c) FeTiO<sub>3</sub>. Black solid, blue solid, and red dashed line represent the experimental data, Voigt function, and fitting result, respectively.

in the main line is  $I_1/I_2 = 1.20, 3.92, 4.38$  for CoO, Fe<sub>2</sub>O<sub>3</sub>, and FeTiO<sub>3</sub>, respectively. The larger  $I_1/I_2$  for FeTiO<sub>3</sub> compared with Fe<sub>2</sub>O<sub>3</sub> supports the statement in Sec. D that the nonlocal-screening effect is more effective in Fe<sub>2</sub>O<sub>3</sub>.

- 
- [1] M. Imada, A. Fujimori, and Y. Tokura, *Rev. Mod. Phys.* **70**, 1039 (1998).
- [2] D. I. Khomskii, *Transition Metal Compounds* (Cambridge University Press, 2014).
- [3] K. Kobayashi, *Nucl. Instrum. Methods. Phys. Res. A.* **601**, 32 (2009).
- [4] M. Taguchi, Y. Takata, and A. Chainani, *J. Electron. Spectrosc. Relat. Phenom.* **190**, 242 (2013).
- [5] M. Taguchi and G. Panaccione, “Depth-dependence of electron screening, charge carriers and correlation: Theory and experiments,” in *Hard X-ray Photoelectron Spectroscopy (HAXPES)*, edited by J. C. Woicik (Springer International Publishing, Cham, 2016) pp. 197–216.
- [6] F. de Groot and A. Kotani, *Core Level Spectroscopy of Solids* (CRC Press, 2014).
- [7] M. A. van Veenendaal and G. A. Sawatzky, *Phys. Rev. Lett.* **70**, 2459 (1993).
- [8] M. van Veenendaal, *Phys. Rev. B* **74**, 085118 (2006).
- [9] A. Hariki, T. Uozumi, and J. Kuneš, *Phys. Rev. B* **96**, 045111 (2017).
- [10] K. Horiba, M. Taguchi, A. Chainani, Y. Takata, E. Ikenaga, D. Miwa, Y. Nishino, K. Tamasaku, M. Awaji, A. Takeuchi, M. Yabashi, H. Namatame, M. Taniguchi, H. Kumigashira, M. Oshima, M. Lippmaa, M. Kawasaki, H. Koinuma, K. Kobayashi, T. Ishikawa, and S. Shin, *Phys. Rev. Lett.* **93**, 236401 (2004).
- [11] M. Taguchi, M. Matsunami, Y. Ishida, R. Eguchi, A. Chainani, Y. Takata, M. Yabashi, K. Tamasaku, Y. Nishino, T. Ishikawa, Y. Senba, H. Ohashi, and S. Shin, *Phys. Rev. Lett.* **100**, 206401 (2008).
- [12] R. Eguchi, M. Taguchi, M. Matsunami, K. Horiba, K. Yamamoto, Y. Ishida, A. Chainani, Y. Takata, M. Yabashi, D. Miwa, Y. Nishino, K. Tamasaku, T. Ishikawa, Y. Senba, H. Ohashi, Y. Muraoka, Z. Hiroi, and S. Shin, *Phys. Rev. B* **78**, 075115 (2008).
- [13] M. Obara, A. Sekiyama, S. Imada, J. Yamaguchi, T. Miyamachi, T. Balashov, W. Wulfhekel, M. Yabashi, K. Tamasaku, A. Higashiya, T. Ishikawa, K. Fujiwara, H. Takagi, and S. Suga, *Phys. Rev. B* **81**, 113107 (2010).
- [14] N. Kamakura, M. Taguchi, A. Chainani, Y. Takata, K. Horiba, K. Yamamoto, K. Tamasaku, Y. Nishino, D. Miwa, E. Ikenaga, M. Awaji, A. Takeuchi, H. Ohashi, Y. Senba, H. Namatame, M. Taniguchi, T. Ishikawa, K. Kobayashi, and S. Shin, *Europhys Lett.* **68**, 557 (2004).



- [15] A. Hariki, Y. Ichinozuka, and T. Uozumi, J. Phys. Soc. Jpn. **82**, 043710 (2013).
- [16] M. Taguchi, A. Chainani, K. Horiba, Y. Takata, M. Yabashi, K. Tamasaku, Y. Nishino, D. Miwa, T. Ishikawa, T. Takeuchi, K. Yamamoto, M. Matsunami, S. Shin, T. Yokoya, E. Ikenaga, K. Kobayashi, T. Mochiku, K. Hirata, J. Hori, K. Ishii, F. Nakamura, and T. Suzuki, Phys. Rev. Lett. **95**, 177002 (2005).
- [17] C. F. Chang, T. C. Koethe, Z. Hu, J. Weinen, S. Agrestini, L. Zhao, J. Gegner, H. Ott, G. Panaccione, H. Wu, M. W. Haverkort, H. Roth, A. C. Komarek, F. Offi, G. Monaco, Y.-F. Liao, K.-D. Tsuei, H.-J. Lin, C. T. Chen, A. Tanaka, and L. H. Tjeng, Phys. Rev. X **8**, 021004 (2018).
- [18] P. Miedema, F. Borgatti, F. Offi, G. Panaccione, and F. de Groot, J. Electron. Spectrosc. Relat. Phenom. **203**, 8 (2015).
- [19] J. Rubio-Zuazo, A. Chainani, M. Taguchi, D. Malterre, A. Serrano, and G. R. Castro, Phys. Rev. B **97**, 235148 (2018).
- [20] A. E. Bocquet, T. Mizokawa, T. Saitoh, H. Namatame, and A. Fujimori, Phys. Rev. B **46**, 3771 (1992).
- [21] M. W. Haverkort, M. Zwierzycki, and O. K. Andersen, Phys. Rev. B **85**, 165113 (2012).
- [22] A. Hariki, M. Winder, and J. Kuneš, Phys. Rev. Lett. **121**, 126403 (2018).
- [23] J. Lüder, J. Schött, B. Brena, M. W. Haverkort, P. Thunström, O. Eriksson, B. Sanyal, I. Di Marco, and Y. O. Kvashnin, Phys. Rev. B **96**, 245131 (2017).
- [24] M. Calandra, J. P. Rueff, C. Gougoussis, D. Céolin, M. Gorgoi, S. Benedetti, P. Torelli, A. Shukla, D. Chandris, and C. Brouder, Phys. Rev. B **86**, 165102 (2012).
- [25] P. Blaha, K. Schwarz, G. Madsen, D. Kvasnicka, and J. Luitz, *WIEN2k, An Augmented Plane Wave + Local Orbitals Program for Calculating Crystal Properties (Karlheinz Schwarz, Techn. Universitat Wien, Austria, 2001), ISBN 3-9501031-1-2*.
- [26] A. A. Mostofi, J. R. Yates, G. Pizzi, Y.-S. Lee, I. Souza, D. Vanderbilt, and N. Marzari, Comput. Phys. Commun. **185**, 2309 (2014).
- [27] J. Kuneš, R. Arita, P. Wissgott, A. Toschi, H. Ikeda, and K. Held, Comput. Phys. Commun. **181**, 1888 (2010).
- [28] M. Karolak, G. Ulm, T. Wehling, V. Mazurenko, A. Poteryaev, and A. Lichtenstein, J. Electron. Spectrosc. Relat. Phenom. **181**, 11 (2010).
- [29] In the LDA+DMFT calculation, the self-energy depends on the spin in the AF phase.
- [30] A. Georges, G. Kotliar, W. Krauth, and M. J. Rozenberg, Rev. Mod. Phys. **68**, 13 (1996).
- [31] G. Kotliar, S. Y. Savrasov, K. Haule, V. S. Oudovenko, O. Parcollet, and C. A. Marianetti, Rev. Mod. Phys. **78**, 865 (2006).
- [32] P. Werner, A. Comanac, L. de' Medici, M. Troyer, and A. J. Millis, Phys. Rev. Lett. **97**, 076405 (2006).
- [33] E. Gull, A. J. Millis, A. I. Lichtenstein, A. N. Rubtsov, M. Troyer, and P. Werner, Rev. Mod. Phys. **83**, 349 (2011).
- [34] L. Boehnke, H. Hafermann, M. Ferrero, F. Lechermann, and O. Parcollet, Phys. Rev. B **84**, 075145 (2011).
- [35] H. Hafermann, K. R. Patton, and P. Werner, Phys. Rev. B **85**, 205106 (2012).
- [36] X. Wang, E. Gull, L. de' Medici, M. Capone, and A. J. Millis, Phys. Rev. B **80**, 045101 (2009).
- [37] M. Jarrell and J. Gubernatis, Phys. Rep. **269**, 133 (1996).
- [38] E. Stavitski and F. M. de Groot, Micron **41**, 687 (2010).
- [39] M. Matsubara, T. Uozumi, A. Kotani, and J. Claude Parlebas, J. Phys. Soc. Jpn. **74**, 2052 (2005).
- [40] J. Sugar, Phys. Rev. B **5**, 1785 (1972).
- [41] A. Tanaka and T. Jo, J. Phys. Soc. Jpn. **61**, 2040 (1992).
- [42] F. M. F. de Groot, J. C. Fuggle, B. T. Thole, and G. A. Sawatzky, Phys. Rev. B **42**, 5459 (1990).
- [43] R. D. Cowan, *The Theory of Atomic Structure and Spectra (University of California Press, Berkeley, 1981), ISBN 0520038215*.
- [44] D. S. Ginley and M. A. Butler, Journal of Applied Physics **48**, 2019 (1977).
- [45] In the present study, we neglect the small off-diagonal elements of  $V^2(\epsilon)$ .
- [46] T. Uozumi, K. Okada, A. Kotani, Y. Tezuka, and S. Shin, J. Phys. Soc. Jpn. **65**, 1150 (1996).
- [47] T. Uozumi, K. Okada, A. Kotani, R. Zimmermann, P. Steiner, S. Hfner, Y. Tezuka, and S. Shin, J. Electron. Spectrosc. Relat. Phenom. **83**, 9 (1997).
- [48] For simplicity, octahedral symmetry is assumed and the effect of long-distance hopping (nonlocal screening) is not taken into account in the qualitative discussion.
- [49] A. E. Bocquet, T. Mizokawa, K. Morikawa, A. Fujimori, S. R. Barman, K. Maiti, D. D. Sarma, Y. Tokura, and M. Onoda, Phys. Rev. B **53**, 1161 (1996).
- [50] R. A. Bair and W. A. Goddard, Phys. Rev. B **22**, 2767 (1980).
- [51] E. Collart, A. Shukla, J.-P. Rueff, P. Leininger, H. Ishii, I. Jarrige, Y. Q. Cai, S.-W. Cheong, and G. Dhalenne, Phys. Rev. Lett. **96**, 157004 (2006).
- [52] H. Tolentino, M. Medarde, A. Fontaine, F. Baudet, E. Dartyge, D. Guay, and G. Tourillon, Phys. Rev. B **45**, 8091 (1992).
- [53] Z. Y. Wu, D. C. Xian, T. D. Hu, Y. N. Xie, Y. Tao, C. R. Natoli, E. Paris, and A. Marcelli, Phys. Rev. B **70**, 033104 (2004).
- [54] D. A. Shirley, Phys. Rev. B **5**, 4709 (1972).